Crowding, Intermolecular Interactions, and Shear Flow Effects in the Diffusion Model of Chemical Reactions

Alessio Zaccone,*,†,§ Nicolas Dorsaz,‖ Francesco Piazza,⊥ Cristiano De Michele,¶ Massimo Morbidelli,† and Giuseppe Foffi‡

†Chemistry and Applied Biosciences, ETH Zurich, CH-8093 Zürich, Switzerland

‡Institute of Theoretical Physics, Ecole Polytechnique Federale de Lausanne, 1015 Lausanne, Switzerland

§Cavendish Laboratory, University of Cambridge, JJ Thomson Avenue, Cambridge CB3 0HE, United Kingdom

‖Department of Chemistry, University of Cambridge, Lensfield Road, Cambridge CB2 1EW, United Kingdom

⊥Centre de Biophysique Moléculaire (CBM-CNRS), Rue Charles Sadron, 45071 Cedex 2 Orleans, France

¶Department of Physics, University of Rome "La Sapienza", Piazzale Aldo Moro 2, I-00185 Roma, Italy

ABSTRACT: In the diffusion model of chemical reactions, the encounter (reaction) rate between reactant particles is governed by the Smoluchowski equation, which is a diffusion equation in a field of forces. We consider crowded environments where the particles diffuse through a "liquid" of like particles. Assuming that the liquid-like short-range structure around the reactant gives rise to an effective (osmotic) barrier leads us to map a complicated many-body problem to a one-dimensional problem. This allows us to describe theoretically such complex systems that are encountered in many applications where crowding, intermolecular interactions, and flow are simultaneously present. A particularly important effect is discovered which is due to the interplay between shear and crowding. This effect is responsible for unexpected peaks in the reactivity at low flow intensity which may explain, among other things, the bizarre colloidal stability behavior of concentrated protein suspensions.
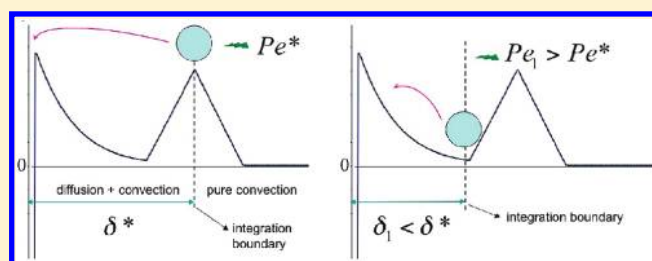
I. INTRODUCTION

Complex fluids and soft matter systems (e.g., colloids, polymers, emulsions) in general are intrinsically characterized by the coexistence of microscopic (atomic, molecular level) and mesoscopic (e.g., macromolecular or colloidal level) processes with different dynamics and relaxation times.[1] The mesoscopic level is the one that eventually determines the macroscopic properties and evolution and is characterized by much slower dynamics and relaxation than the atomic level of the embedding fluid. This is such a general feature that *slow dynamics* can be used as an equally good definition of soft matter in alternative to or besides the notion of mechanical fragility. In any kind of application, one is interested in knowing, and possibly predicting, the time-evolution of the system which is in turn related to the time scales of microscopic physical processes.

The great range of length and time scales spanned represents the most fundamental aspects of soft matter. As a consequence, it is clear that any physical modeling has to be based on this intrinsic multiscale aspect of soft matter. In this sense, coarse-graining over the degrees of freedom of the short length and fast time scales is a necessary step. This coarse-graining is of vital importance in order to achieve the mathematical simplification required by the methods of physics. This approach is equally useful for static as well as dynamic properties of soft-matter systems. It must be stressed, however, that this way of dealing

with complexity has not simply the goal of tackling problems that would be otherwise impossible to solve. This reductive approach is of great help in pinpointing the relevant properties of soft-matter systems. One of the most successful routes to the modeling of soft matter is to derive an effective interaction that allows one to restrict the description to the mesoscopic level and to make predictions for the macroscopic properties (for a review, see ref 2). For a colloidal system, this approach allows one to treat colloids as "designer atoms"[3] and to use the tools of statistical mechanics to predict and describe new unexpected phenomena. For dynamical properties, a similar idea of coarse-graining can be applied to the relevant time scales, and although it presents some serious challenges,[4] it can be of great help in modeling.

In this paper, we will focus mainly on the dynamical coarse grain. Coarse-graining of this type stems directly from the seminal works on Brownian motion by Einstein and Smoluchowski.[5,6] Einstein[5] derived the famous formula for the mean squared displacement of colloidal particles, $\bar{s}^2 = 2dDt = 2d(kT/b)t$, by doing just the same coarse-graining: the degrees of freedom of the molecules of solvent are integrated out by treating the latter as a continuum endowed with a temperature T and

exerting a (Stokes) friction b. This clearly makes sense only if the mean free path of the surrounding molecules is small in comparison with that of the particles. This is already the case if our particle is a protein of a few nanometers of diameter or any synthetic or biological polymer molecule in solution with a number of monomeric units $N_m > 1000$.

At a higher level, the dynamics of the particles is described by the Smoluchowski equation.[7,8] This is a partial differential equation of motion for the probability density function of the Brownian particles that is valid in the *overdamped* limit where the particles' momenta are already at equilibrium with the thermal bath of the solvent at a time $t \ll m/b$, where m is the particle mass.[7] Also hydrodynamics can be incorporated within the Smoluchowski description, with various degrees of approximation.[8,9] A rigorous theory would require that one works with the N-particle Smoluchowski equation.[8] A very promising way to manage the latter by keeping the treatment at a semianalytical level is the use of density functional theory.[10,11] However, including nontrivial external forces or microscopic effective interactions poses several unresolved challenges.

On the other hand, phenomenology can inspire meaningful manipulations that enable one to treat collective effects as well as external fields and complex interactions still within an *effective* one-dimensional Smoluchowski equation. Analytical solutions to the latter can be attempted by exploiting the symmetries of the problem. In this situation, it is possible to derive a statistical description in terms of the (partial differential) equation of motion of the probability density function of positions of the particles, which goes under the name of the Smoluchowski equation. In fact, this is a special case of the more general Fokker—Planck equation, whose solution is the probability distribution of the phase space coordinates of a system.[12]

In this paper, we are going to discuss some possible routes to develop the phenomenological approach to the aggregation/reaction problem in crowding and shear within the Smoluchowski framework. To this aim we will begin with a self-contained introduction to this approach and we will highlight recent results obtained in the application to different problems within the realm of soft matter. The second part of the paper is organized as follows. In section II, we review a recently proposed approach to evaluate the rate coefficient of the classical Smoluchowski rate in the presence of crowding. In this framework, we present some new analytical results and we apply them to the case of real nanoparticles. In section III, we extend the theory to the case of shear and an analytical solution is found in this case, too. In the Conclusion, we speculate on the possible experimental implication of our theory and we speculate on its future extensions.

II. REACTION RATES IN CROWDED BROWNIAN SYSTEMS

A. Diffusion-Limited Aggregation/Reaction Kinetics: Analytical Theory. As shown in the Appendix, the Smoluchowski equation, which describes a free Brownian particle moving within an external potential,[13,14] reads as

$$\frac{\partial \rho}{\partial t} = \frac{1}{b} \left[\nabla \cdot (-\mathbf{K}(\mathbf{x})\rho + kT\nabla\rho) \right] \quad (1)$$

where ρ denotes the particle probability density function, $\mathbf{K}(\mathbf{x})$ the force field, and b the Stokes friction. As shown in the Appendix, for this one-dimensional case analytical expressions can be derived for aggregation and escape rates. Now the

question is if simple analytical expressions can be derived also in the case of non-negligible density of Brownian particles in the system, possibly without resorting to the N-particle Smoluchowski equation framework (described in the Appendix).

The problem of many-body effects on the rate of chemical reactions within the diffusion model is a long-standing one and various theoretical approaches have been proposed in the past (see, for example, ref 15 for a review). In the present work we are interested in the following subcase of the general many-body problem that is schematically depicted in Figure 1. We consider a dense system of identical reacting species that we model as Brownian spheres of radius R_p. These are labeled as particle A in the scheme in Figure 1. Moving in such a "sea" of A-particles is the sink, labeled as particle B in Figure 1, which is also a Brownian sphere of radius R_s. We make the following assumptions in our problem: (i) the sink B represents an absorbing boundary for each of the A-particles, (ii) there are only binary reactions between B and A such that the order of the reaction is 1 with respect to both B and A, and (iii) the A-particles interact among each other as hard spheres or effective hard spheres (the latter case occurs when the A-particles are charged).

Our objective is to find an analytical expression for the encounter (reaction) rate for this problem within the one-particle approximation. We start by recognizing that the high density of A particles brings about the following consequences: (1) the single-particle diffusion for A-particles is increased with respect to the dilute case due to the collective motion and due to the presence of osmotic pressure gradients, but it is decreased due to many-body hydrodynamic interactions (HI), and (2) the diffusive transport toward B is affected by the liquid-like structure of the A-particles around B. In the course of this work we refer to this second effect as "crowding".

We describe effect 1 on the single-particle diffusion following Dzubiella and McCammon[16] and neglecting many-body HI for the moment. What one needs to do, first of all, is to introduce a collective diffusion coefficient that accounts for density effects on the diffusion of a Brownian particle moving in a homogeneous substrate of like particles that mutually interact as hard spheres (HS). Such a generalized Stokes—Einstein coefficient is given by $D(\rho) = M(\rho) \, d\Pi(\rho)/d\rho$.[16] $M(\rho)$ is the generalized mobility and accounts for the HI that are due to the motions of the other particles and are transmitted to the tagged particles through the solvent.[8] It is given by $bH(k)$, where $H(k)$ is the hydrodynamic mobility function (k is the wave-vector) which accounts for the effect of hydrodynamic interactions. When HI are neglected, $M(\rho) \rightarrow b^{-1}$. The factor $d\Pi(\rho)/d\rho$ accounts for the increased mobility due to diffusion down an osmotic pressure gradient.[8,16] In the absence of external fields ($K = 0$) and under account of collective diffusion, the stationary Smoluchowski equation, eq 1, can be rewritten in spherical coordinates as follows[16]

$$\frac{b^{-1}}{r^2} \frac{\partial}{\partial r} \left(r^2 \frac{\partial \rho}{\partial r} \frac{\partial \Pi}{\partial \rho} \right) = 0 \quad (2)$$

Integration of this equation with the absorbing boundary condition, $\rho(0) = 0$, and the far field boundary condition, $\rho = \rho_\infty$ at $r = \infty$, as discussed in the Appendix, gives[21]

$$\kappa = \kappa_S \frac{1}{kT} \frac{\Pi(\rho_\infty)}{\rho_\infty} \quad (3)$$

where $\kappa_S = 4\pi R D' \rho_\infty$ is the Smoluchowski rate for diffusion-limited reaction/aggregation at infinite dilution. $\beta[\Pi(\rho_\infty)/\rho_\infty]$ is
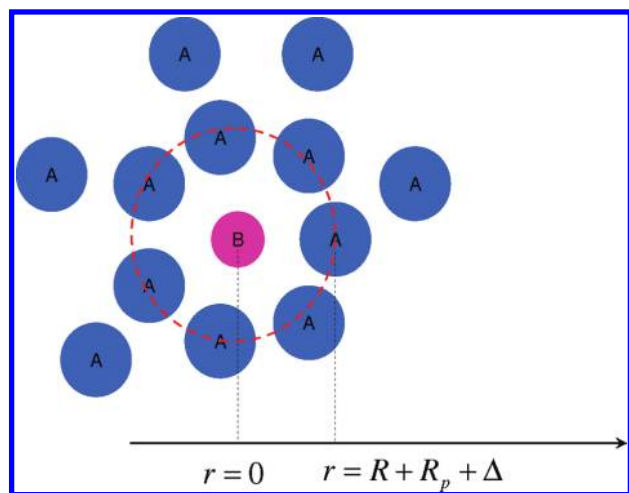
Figure 1. Schematic representation of the crowding of reactant species (A) around the sink (B). The dashed circle corresponds to the first coordination shell in the radial distribution function.

Figure 2. Schematic of the edge-shaped potential used to model the crowding.

equal to the compressibility factor Z of the system, and in terms of the volume fraction of particles, $\phi = (4/3)\pi R_p^3 \rho_\infty$, can be given for HS by the Carnahan–Starling equation:[17] $Z(\phi) = (1 + \phi + \phi^2 - \phi^3)/(1 - \phi)^3$ for $\phi \lesssim 0.4$. For higher concentrations the Hall equation of state in the fluid branch can be used, which employs up to seven virial coefficients.[18] Because the compressibility Z is a monotonically increasing function of the density (or volume fraction $\phi = 4\pi R_p^3 \rho_\infty/3$), it is evident that the reaction rate with a tagged particle/sink as it is given by eq 19 is also a monotonically increasing function of ρ_∞ and ϕ.

All this holds true as long as the distribution of Brownian particles in the system is spatially homogeneous everywhere with the only exception being the region around the sink, where the absorbing boundary causes local depletion of particles, $\rho(r) = \rho_\infty[1 - (R/r)]$, with the contact radius $R = R_s + R_p$. This holds true in HS systems for $\phi \lesssim 0.1$. At larger packing fractions, it is well-known that excluded-volume effects cause the local number density at r, $\rho(r)$, around a tagged particle at the origin (the sink in our case) to depart significantly from the macroscopic number density ρ_∞.[17] This is the short-range order characteristic of the liquid state, which is manifest in the pronounced nearest-neighbor peak of the radial distribution function, the latter defined as $g(r) = \rho(r)/\rho_\infty$.[17] With reference to our scheme in Figure 1 the peak in the $g(r)$ corresponds to the dashed circle. This is what we referred to above as crowding and is listed as effect 2. Such short-range correlations in the structure of liquids, and the corresponding peaks in the $g(r)$, die out typically over distances on the order of several particle diameters, which means that $\rho(r)$ is not at all flat and equal to ρ_∞ in the neighborhood of the sink. Since the latter region is clearly the most important from the point of view of the kinetic processes we are interested in, it is necessary to take into account the short-range structure around the reactant particle. Event-driven Brownian dynamics (EDBD) simulations[19,20] have been employed to study the effects of crowding and of the liquid-like short-range structure on diffusion-limited reaction rates.[21] It was found indeed that the theory given by eq 3 is able to capture the density dependence of κ only in the limit of a sink size much larger than the background particles. If the tagged particle is of a size comparable with that of the other particles, eq 3 cannot
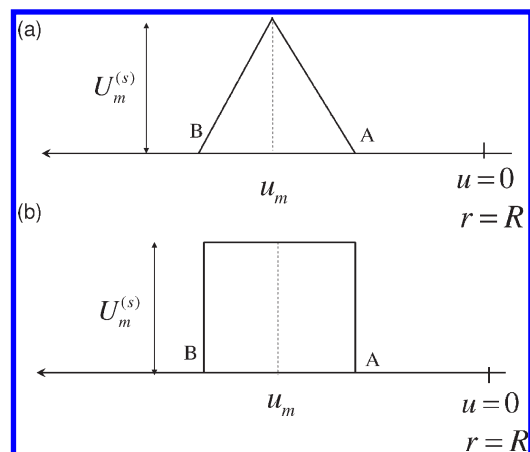
account for the significant decrease of $d\kappa/d\phi$ as a function of ϕ that is evident for $\phi \gtrsim 0.3$. The discrepancy becomes even more pronounced upon decreasing the ratio R_s/R_p, where R_s is the tagged particle/sink size. The latter effect can be understood as a slowing down of the kinetics upon increasing ϕ due to the increasing frustration experienced by the particles around the first coordination shell that are in mutual competition to react with the sink.[21] In general, the locally higher density within the first coordination shell [corresponding to the first peak in the $g(r)$] gives rise to an adverse local gradient in the osmotic pressure associated with an effective local resistance to the diffusive transport (since particles have to diffuse "uphill" the osmotic gradient in order to have access to the sink).

Motivated by the recent findings of some of us,[21] we use the following heuristic "toy model" to represent the effect of crowding. First of all, for perfectly spherical hard spheres the barrier around the sink due to the crowding can be reasonably assumed to be isotropic around the sink and thus may be modeled by means of a centrally symmetric *effective potential*. In the spirit of diagrammatic expansion of effective potentials between big particles in a sea of small particles,[22] we make the following ansatz for the effective potential:

$$\beta U^{(s)} = \beta U_0(\phi) + \beta U_2^{(s)}(r; \phi, R_s/R_p) \tag{4}$$

where the term $U_0(\phi)$ is reminiscent of effective potential *volume term*,[2] the term $U_2^{(s)}(r; \phi, R_s/R_p)$ is analogous to the second order term in the expansion, and $\beta = 1/kT$. The height of the term $U_2^{(s)}$ can be reasonably taken to be proportional to the local excess osmotic pressure with respect to ideality, by assuming that ideality locally holds in the depleted shell of the radial distribution function,

$$\beta U_2^{(s)} = h(r)c\frac{\Pi(\rho_\Delta) - \Pi_{id}}{\Pi_{id}} = h(r)c[Z(\rho_\Delta) - 1] \tag{5}$$

where $h(r)$ is a generic function that depends only on r, where $\rho_\Delta = \rho_\Delta(\phi, R_s/R_p)$ is related to the Smoluchowski density at the radial coordinate of the first peak, while $\Pi_{id} = \beta\rho$. The superscript (s) indicates that this effective potential accounts for the effect of structure on the kinetics. c is a numerical proportionality constant that, for the case of hard spheres, was determined in ref 21 by comparison with the simulations. Therefore $U_2^{(s)}(\phi, R_s/R_p)$ is a function of the density of the system and of the size of the

tagged reactant with respect to the background particles. Reasonable shapes of $U_2^{(s)}$ are shown in Figure 2. Using eqs 4, 21, and 10 one obtains

$$\kappa = \kappa_S e^{-\beta U_0} \left(R \int_R^\infty \frac{e^{\beta U_2^{(s)}}}{r^2}\, dr \right)^{-1} \qquad (6)$$

For large values of sink size, i.e., $R_s/R_p \to \infty$, or low volume fractions, $U_2^{(s)}$ can be neglected, i.e., $U_2^{(s)} \approx 0$, and eq 6 must reduce to eq 4; as a result the following equality holds

$$e^{-\beta U_0(\phi)} = \beta Z(\phi)$$

so that eq 6 can be rewritten as follows:

$$\kappa = \kappa_S \beta Z(\phi) \left(R \int_R^\infty \frac{e^{\beta U_2^{(s)}}}{r^2}\, dr \right)^{-1} \qquad (7)$$

1. Edge-Shaped Osmotic (Crowding) Barrier. The actual shape of the structural or osmotic pseudopotential $U_2^{(s)}$ is presumably dictated by the radial profile of the local osmotic pressure near the sink, $\Pi(\rho(r))$. As this remains unknown, we can only reasonably assume that the barrier is peaked approximately near the depleted shell of the radial distribution function, where it goes through its maximum as given by eq 5. Without knowing the functional shape of the barrier, we can still examine two limiting cases, i.e. the square-shaped barrier and the edge-shaped barrier. The actual barrier will presumably have some shape comprised between these two limits. Let us start by examining the case of an edge-shaped barrier, schematically represented as the edge-shaped function in Figure 2a peaked near the radial coordinate corresponding to the first depletion shell in the radial distribution function, i.e., at $r = R + R_p + \Delta$ where $\Delta = 2R_p/3$ (cf. Figure 1 for the position of the peak) and $R = R_s + R_p$. We now introduce the rescaled variable $u = r/R - 1$. Since r is the center-to-center distance, we have that the position of the maximum is $r_m = (5/3)R_p + R$ from which we have $u_m = (5/3)R_p/R$.

With reference to Figure 2a, in the neighborhood of the cusp we have $U_2^{(s)} \approx U_m^{(s)} - \omega(u - u_m)$. We want to evaluate the integral $R \int_R^\infty (\exp\, U_2^{(s)})/r^2\, dr = \int_0^\infty (\exp\, U_2^{(s)})/(u+1)^2\, du \approx 1/(u_m+1)^2 \int_0^\infty \exp\, U_2^{(s)}\, du$. The integral $\int_0^\infty \exp\, U_2^{(s)}\, du$ can be approximated with $2\int_0^\infty \exp[U_m^{(s)} - \omega(u-u_m)]\, d(u - u_m)$, which is twice the contribution coming from the rectangular triangle, which represents the half of the whole triangle in Figure 2a.[13] Therefore, we obtain

$$\frac{2}{(u_m+1)^2} \int_0^\infty \exp[U_m^{(s)} - \omega(u - u_m)]\, d(u - u_m)$$

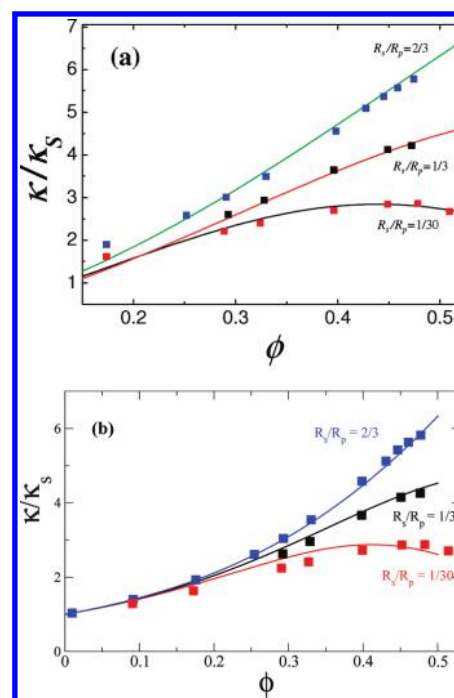$$= \frac{2kT}{\omega(u_m+1)^2} \exp[U_m^{(s)}/kT] \qquad (8)$$

Substituting $\omega = U_m^{(s)}/u_m$ and using eq 5 we finally get

$$\frac{\kappa}{\kappa_S} \approx \frac{(u_m+1)^2}{2u_m} Z(\phi_\infty) c e^c [Z(\phi_\Delta) - 1] e^{-cZ(\phi_\Delta)} \qquad (9)$$

where we used $U_m^{(s)}/kT = c[Z(\phi_\Delta) - 1]$.

Equation 9 can be compared with the simulations. To evaluate ϕ_Δ we use

$$\phi_\Delta = A\phi_S(r_\Delta) = A\phi_\infty[1 - (R/r_\Delta)] \qquad (10)$$

Figure 3. Theoretical curves for the diffusion-limited reaction rate under crowding, considering (a) an edge-shaped barrier (eq 12) and (b) a square-shaped barrier (eq 13) at different values of the R_s/R_p ratio. Symbols are EDBD simulations from ref 21 for the same conditions.

where $\phi_S(r) = \phi_\infty[1 - (R/r)]$ is the Smoluchowski (infinite-dilution) profile and A is a numerical constant that accounts for the short-ranged liquid structure that is absent in the dilute limit. Further we have that $r_\Delta = R + \Delta = R + (2/3)R_p = R_s + (5/3)R_p$. Recalling that $u_m = (5/3)R_p/R$, we have

$$\frac{(u_m+1)^2}{2u_m} \approx 2 \qquad (11)$$

We find that the simulation data of ref 21 for three different values of the ratio R_s/R_p can all be fitted with the values $A \approx 1.12$ and $c = 2.1$. The value of the constant c is somewhat different from the one ($c = 3.75$) obtained in ref 21 from the comparison with the simulations. The comparison is shown in Figure 3. As one can see, the approximate closed-form expression, eq 9, is able to reproduce the simulation results rather well.

Equation 9 is more accurate when the edge-shaped crowding barrier is significantly steep, i.e. for $\phi > 0.2$ and for large values of the ratio $U_m^{(s)}/u_m$, which corresponds to large values of R_s/R_p. On the other hand, it is less accurate at low ϕ, where the barrier vanishes and the steepest-descent approximation is no longer valid. The correction factor due to the crowding osmotic barrier caused by the liquid short-range structure and defined by the relation $C_s = \kappa/\kappa_S \beta Z(\phi)$ in this case is given by

$$C_s = \frac{(u_m+1)^2}{2u_m} c e^c [Z(\phi_\Delta) - 1] e^{-cZ(\phi_\Delta)} \qquad (12)$$

which has been plotted in Figure 4 as a function of the total packing fraction ϕ.

Since eq 9 is valid only for high effective barriers[13] and therefore for significant crowding (i.e., for significant structuring around the sink), the correction is shown only for $\phi \geq 0.2$. It is clearly seen that in the range of interest C_s is a decreasing
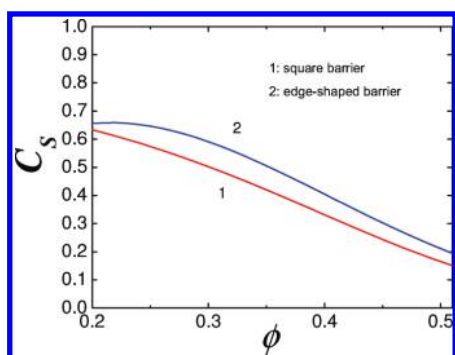
Figure 4. The correction to the diffusion-limited kinetic constant due to the crowding as a function of the volume fraction of particles, according to eq 12 (edge barrier) and eq 13 (square barrier), calculated for $R_s/R_p = 1/30$.

function of ϕ. Hence, the theory predicts that crowding due to the short-range liquid structure can significantly slow down the reaction/aggregation kinetics.

2. Square-Shaped Osmotic (Crowding) Barrier. In the case of a square-shaped barrier, depicted schematically in Figure 2b, the reaction rate under crowding, eq 7, can be evaluated exactly. This leads to a correction factor

$$C_s = \left[(e^{\beta U_2^{(s)}} - 1)\left(\frac{1}{R^-} - \frac{1}{R^+}\right) + \left(\frac{1}{R}\right) \right]^{-1} \quad (13)$$

with $R^- = r_\Delta + R_p/2$ and $R^+ = R^- + R_p$. The height of the energy barrier induced by crowding is assumed to be proportional to the excess osmotic pressure at the first coordination shell $U_2^{(s)} = h(r_m)c[Z(\phi_\Delta) - 1]$, as explained above. The R_s/R_p dependence of the reaction rate is then introduced via the Smoluchowski dependence of the density at r_Δ [$\phi_\Delta \equiv \phi_S(r_\Delta)$]. It seems indeed that the $(R_p + R_s)^{-1}$ dependence of the ideal Smoluchowski case is also underlying the crowded case by weighting somehow the competition between the diffusing particles in the vicinity of the sink. A one-parameter fit of

$$\kappa = \kappa_s \beta Z(\phi) \, C_s(\phi, R_s, R_p) \quad (14)$$

to the numerical results accounts particularly well for both the ϕ and the R_s/R_p dependence of the rate ($c = 2.45$).

3. Comparison between the Two Limiting Barrier Profiles. The correction factors calculated analytically for the square and for the edge barrier can be compared in Figure (4). The two functions are very similar both qualitatively and quantitatively. In the case of the square barrier, the result for C_s is exact and therefore the function is able to recover the Smoluchowski rate, in the $\phi \rightarrow 0$ limit. This is not possible in the case of the edge-shaped barrier, because of the already mentioned steepest-descents approximations, which fails for a vanishing height of the barrier $U_m^{(s)}$.

We conclude, from this comparison and from the consideration of Figure (3), that both barrier shapes yield reasonably good results for the rate in good comparison with the simulation results. This implies that the true crowding barrier must have some functional form in between the two limiting shapes considered here.

4. Remarks on the Nonmonotonic Dependence of the Rate upon the Packing Fraction. It is interesting to study the conditions under which the reaction/aggregation rate becomes nonmonotonic as a function of the global density ϕ and thus the

possibility of having regimes where $d\kappa/d\phi < 0$. From eq 12 we have that

$$\frac{d(\kappa/\kappa_S)}{d\phi} \propto [Z(\phi) \, C_s'(\phi) + Z'(\phi) \, C_s(\phi)] \quad (15)$$

where $C_s'(\phi) = dC_s/d\phi < 0$ and $Z'(\phi) = dZ/d\phi > 0$. Hence the ϕ values where the condition

$$|Z(\phi) \, C_s'(\phi)| > Z'(\phi) \, C_s(\phi) \quad (16)$$

is satisfied, correspond to a situation where upon increasing ϕ the enhanced diffusive transport due to collective diffusion (proportional to $Z'(\phi) > 0$) is no longer able to balance the slow-down in the transport due to the crowding (proportional to $C_s'(\phi) < 0$). Equation 16 allows one to estimate at glance the range of ϕ where an increase in the density becomes detrimental for the efficiency of the diffusive transport to the target molecule.

5. Activated Hopping with Crowding. Equation 9 describes a kinetic process that is controlled by the escape rate across an energy barrier. As the form of eq 9 suggests, the crowding around the reactant acts as an effective osmotic barrier that the incoming particle has to cross. The crossing rate, just as in the case of Kramers[13] rate discussed in the Appendix, is an exponentially decreasing function of the (in this case, osmotic) barrier height. The latter, in turn, is proportional to the local compressibility in the first-coordination shell around the target molecule/sink. Finally, eq 9 shows that the rate in the presence of crowding is the result of the competition between two competing phenomena. One is the speed-up in the rate due to the collective diffusion, which is proportional to $Z(\phi)$, thus an increasing function of ϕ, and the other one is the crowding, which ultimately goes as $Z(\phi_\Delta)e^{-Z(\phi_\Delta)}$ and therefore is a decreasing function of ϕ. Clearly the latter effect, being exponential, eventually prevails, thus determining an overall decreasing trend of the reaction rate with ϕ, which sets in after reaching a maximum in the kinetic rate. The location of the maximum is determined by the extent of the crowding, i.e., by the ratio R_s/R_p, which in turn controls $Z(\phi_\Delta)$. Upon decreasing R_s/R_p (i.e., increasing the crowding), the maximum gets shifted to lower ϕ values and the slow-down of the kinetics also becomes more dramatic. On the other hand, when the ratio R_s/R_p is increased, it can be shown that the maximum is shifted to higher ϕ values and the dependence of C_s on ϕ gets smeared out.

Hence, the comparison between eq 9, on one hand, and the Kramers rate, eq 48 in the Appendix, on the other, suggests an analogy between thermally activated-rate processes in interaction−potential energy landscapes[13] and the activated hopping in crowded environments[23] in the absence of external or interaction potentials. Also, it supports the legitimacy of treating the "structural" effective potential due to the crowding in complete analogy and on equal footing with intermolecular potentials.

B. Reaction-Limited Aggregation/Reaction Kinetics with Crowding. The above result can be generalized to the presence of medium- and long-range (intermolecular) interactions between the Brownian molecules. In general, large Brownian molecules can interact via a superposition of attractive and repulsive interaction forces.[24,25] This is the case of the well-known Derjaguin−Landau−Verwey−Overbeek (DLVO) interaction potential of colloidal particles which arises from the superposition of attractive van der Waals forces and repulsive electrostatic forces which results in a net interaction energy barrier whenever the ionic strength in the solvent (I) is not

enough to completely screen the Coulomb repulsion.[14,24] The kinetics in this regime, where a finite interaction energy barrier is present, is referred to as "reaction-limited" (RL) kinetics, in contrast to the regime of "diffusion-limited" (DL) kinetics, where there is no interaction energy barrier. In the RL case the stationary kinetics is described by the *effective* Smoluchowski equation

$$\frac{b^{-1}}{r^2} \frac{\partial}{\partial r} r^2 \left(\frac{\partial \rho(r)}{\partial r} \frac{\partial \Pi[\rho(r)]}{\partial \rho(r)} + \frac{\partial U_{\text{eff}}}{\partial r} \rho \right) = 0 \qquad (17)$$

Here we make the further assumption that the superposition principle holds such that the total interaction potential is given by

$$U_{\text{eff}} = U + U_2^{(s)} \qquad (18)$$

U represents the *direct* or intermolecular interaction potential (i.e., the sum of van der Waals, electrostatic, etc.), while $U_2^{(s)}$ represents the additional osmotic potential energy due to the local liquid structure.

It is worth noticing that charged Brownian particles, especially at low ionic strength, behave as their sizes were larger due to the electrostatic repulsion that keeps them apart.[26] Thus, in a system of identical, charged Brownian particles, the effective packing fraction is larger due to this effect and is given by $\tilde{\phi} = (4/3)\pi \tilde{R}_p^3 \rho_\infty$, where $\tilde{R}_p$ is the effective particle radius.[26] The latter is estimated from the condition $U(\tilde{R}_p) \approx kT$. For the A–A interaction in our system, we can assume a screened-Coulomb repulsion that can be estimated using the Yukawa potential $\beta U = \alpha e^{-\kappa_D r}/\kappa_D r$, where κ_D is the inverse of the Debye length $\lambda_D = [(\varepsilon \varepsilon_0 kT)/(2N_A e^2 I)]^{1/2}$, while $\alpha = 4\pi \varepsilon \varepsilon_0 \psi_0^2 R_p^2 \kappa_D e^{2R_p \kappa_D}/kT$ is the screening parameter (ψ_0 is the electrostatic potential on the particle surface and $\varepsilon \varepsilon_0$ is the dielectric constant of the solvent). This yields the following estimate for the effective radius $\tilde{R}_p \approx (2\kappa_D)^{-1} \ln[\alpha/(\ln \alpha)]$.[26] As an example, the effective radius of particles with $R_p = 300$ nm and surface potential $\psi_0 = 0.02$ V in water under low-ionic strength conditions such as $I = 0.1$ mM equivalent to $\lambda_D = \kappa_D^{-1} = 30.4$ nm at room temperature is on the order of 800 nm. Apart from this effect, the Brownian particles can still be treated as Brownian hard spheres with radius $\tilde{R}_p$. Thus, in this case the reaction/aggregation kinetic constant is given by[30]

$$\frac{\kappa}{\kappa_S} = Z(\tilde{\phi}) \left(R \int_R^\infty \frac{\exp\left(\beta U + \beta U_2^{(s)}\right)}{r^2} \, dr \right)^{-1} \qquad (19)$$

Equation 19 gives a theoretical estimate of reaction rates between the charged Brownian A-particles and the sink S under the account of both crowding and interactions and is thus expected to have applications in the field of biochemical reactions in vivo involving charged biomolecules.[27] Due to the linearity of the Smoluchowski equation, the superposition principle is valid and the electrostatic barrier sums up with the effective barrier contributed by the crowding. The height of the latter can be calculated using eq 5 for given ϕ and R_s/R_p. Hence the effect of crowding on the aggregation/reaction kinetics in this case is significant when the height of the *direct* (DLVO) interaction energy barrier is $U_m \lesssim 10kT$. This is the case often encountered in biological systems, where the relatively large ionic strength of the environment leads to electrostatic energy barriers on this order of magnitude.[27] Instead, for highly charged molecules in the low-salt limit typically $U_m \gg 10kT$, so that $U_{\text{eff}} \approx U$ is a good
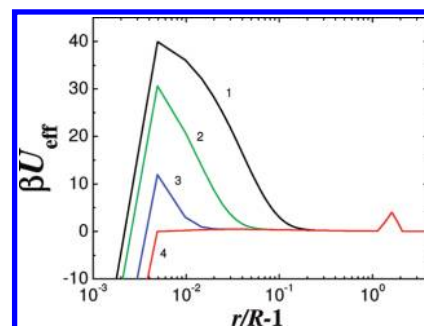
Figure 5. Theoretical curves for the effective interaction potential made of an intermolecular-interaction component of the DLVO type, upon varying ionic strength I, and of the contribution due to the crowding. $R_p = 300$ nm, $R_s = 10$ nm, $\psi_0 = -0.020$ V. (1) $I = 1$ mM, (2) $I = 10$ mM, (3) $I = 100$ mM, and (4) $I = 1000$ mM.

approximation and the effective crowding barrier is small compared to the electrostatic barrier. To illustrate these considerations, we have plotted the net effective potential given by eq 18 when the direct intermolecular part U is calculated for typical particles of two different sizes, $R_p = 300$ nm and $R_p = 30$ nm and $R_s/R_p = 1/30$ in both cases, under conditions of significant crowding corresponding to a packing fraction $\phi = 0.4$. We consider the case where the S–A interaction is represented by the DLVO potential. In Figure 5 effective potentials of the type $U_{\text{eff}} = U^{\text{DLVO}} + U_2^{(s)}$ are plotted for $R_p = 300$ nm and $\psi_0 = -0.02$ V and varying the ionic strength I while the crowding is constant and corresponds to $\phi = 0.4$. The electrolyte concentration controls the range of the electric double layer repulsion through the Debye screening parameter κ_D. As can be seen, the barrier due to crowding is well-separated from the DLVO barrier, which is significantly shorter in range. For the lowest ionic strength considered, the DLVO barrier is much higher than the barrier due to crowding, and the role of the latter is therefore comparatively small. Upon increasing the electrolyte concentration and the ionic strength, the DLVO barrier decreases and thus the crowding barrier becomes comparatively more important. For complete screening of the double layer (curve 4 in the figure), the crowding barrier represents the only repulsive contribution to the total effective potential. Effective potential curves have been calculated also for the case of smaller particles, $R_p = 30$ nm, and are reported in Figure 6. As is well-known, the DLVO theory predicts that the barrier becomes significantly lower upon decreasing the particle size and keeping the ionic strength and surface potential constant. In this case, not only is the height of the crowding barrier always comparable with the height of the DLVO barrier, but the two barriers are also much closer to each other and even merging together in the low I limit. A local minimum is apparent in this case. Hence, the interplay between intermolecular interaction forces between the molecules and the crowding due to excluded-volume can give rise to effective potential profiles that are not at all trivial and therefore can affect the reaction kinetics to a relevant extent. The physical parameters that correspond to the effective potentials shown in Figures 5 and 6 are summarized in Table 1. Theoretical predictions for the reaction-limited kinetics in the presence and in the absence of crowding can be done using eq 19 and are shown in Figures 7 and 8 for the two sets of parameters 1–4 and 5–8 of Table 1, respectively. The values of the kinetic constant calculated in the presence of crowding, i.e., using $U_{\text{eff}} = U^{\text{DLVO}} + U_2^{(s)}$ in the

7388

dx.doi.org/10.1021/jp200439a |*J. Phys. Chem. B* 2011, 115, 7383–7396
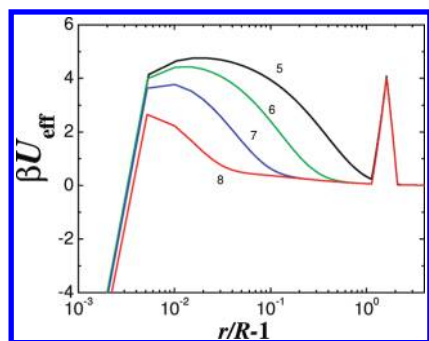
Figure 6. Theoretical curves for the effective interaction potential made of an intermolecular-interaction component of the DLVO type, upon varying electrolyte concentration, and a contribution due to the crowding. R_p = 30 nm, R_s = 1 nm, $\psi_0 = -0.020$ V. (5) I = 1 mM, (6) I = 10 mM, (7) I = 100 mM, (8) I = 1000 mM.

Table 1. Physical Parameters Used for the Computation of the Effective Interaction Potential Curves 1–4 (shown in Figure ⁵) and 5–8 (shown in Figure ⁶)

	ψ_0, V	I, mM	λ_D, nm	R_s/R_p, nm/nm	ϕ
1	−0.02	1	9.61	10/300	0.40
2	−0.02	10	30.4	10/300	0.40
3	−0.02	100	0.96	10/300	0.40
4	−0.02	1000	0.30	10/300	0.40
5	−0.02	1	9.61	1/30	0.40
6	−0.02	10	30.4	1/30	0.40
7	−0.02	100	0.96	1/30	0.40
8	−0.02	1000	0.30	1/30	0.40

Smoluchowski equation, are systematically larger than those without crowding, i.e., using $U_{eff} = U^{DLVO}$, in the high-ionic strength limit, where the electrostatic repulsion is completely screened and the DLVO barrier, U_m^{DLVO}, vanishes. However there is a very significant difference depending upon the size of the particles. For typical colloid-size particles (R_p = 300 nm) there is practically no visible effect induced by the crowding, as long as there exists a nonvanishing DLVO barrier. As one approaches the critical electrolyte concentration that completely screens the DLVO barrier (U_m^{DLVO} = 0) and thus approaches the diffusion-limited fast reaction regime (denoted as DL, to the right of the dashed line in the figures), the effect of the crowding becomes significant and rapidly reaches the constant limit of diffusion-limited kinetics with crowding dealt with in the previous section. On the other hand, we observe that, in the case of nanometer-scale particles (more relevant for biochemical reactions), there is a significant slow-down induced by the crowding already well within the reaction-limited regime where the electrostatic barrier is still significant, i.e., at electrolyte concentrations well below the diffusion-limited regime.

Hence, we conclude that the effect of crowding on the reaction/aggregation rate of nanometer-scale particles can be very important also in the presence of a significant electrostatic barrier. This can be explained with the fact that with smaller particles the relative range of the screened-Coulomb repulsion is comparatively longer and thus can interfere more significantly with the repulsive barrier due to the crowding.
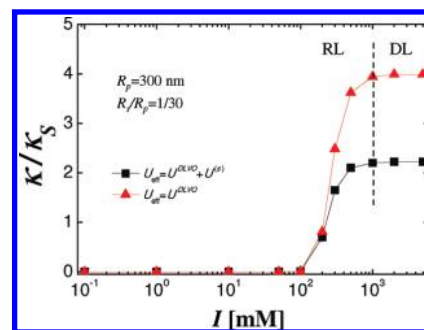
Figure 7. Theoretical curves for the reaction rate in the presence of an effective potential made of an intermolecular DLVO component, upon varying the electrolyte concentration, and a contribution due to the crowding. R_p = 300 nm, R_s = 10 nm. $\psi_0 = -0.020$ V. Triangles, $U_{eff} = U^{DLVO}$; squares, $U_{eff} = U^{DLVO} + U_2^{(s)}$.
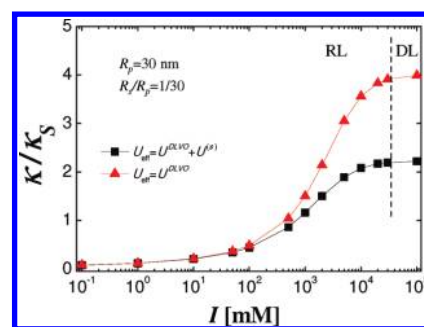
Figure 8. Theoretical curves for the reaction rate in the presence of an effective potential made of an intermolecular DLVO component, upon varying the ionic strength I, and a contribution due to the crowding. R_p = 30 nm, R_s = 1 nm. $\psi_0 = -0.020$ V. Triangles, $U_{eff} = U^{DLVO}$; squares, $U_{eff} = U^{DLVO} + U_2^{(s)}$.

Clearly, biological molecules are very complex entities and describing them in terms of effective colloidal potentials amounts to a substantial coarse-graining. However, the above treatment represents the first theoretical attempt to capture both many-body effects and intermolecular interaction forces within a single and relatively simple physical picture. In the next section we add a further degree of complexity by including the effect of shear flow.

III. REACTION RATES IN CROWDED BROWNIAN SYSTEMS UNDER SHEAR FLOW

A. Theory. If the Smoluchowski equation is the microscopic (stochastic) counterpart of the diffusion equation, the Smoluchowski equation with convection is the microscopic counterpart of the convective diffusion equation.[8,28] The latter governs the probability distribution of a Brownian particle in coordinate space in the presence of both a conservative force field and an externally applied flow. Considering a suspension of spherical particles, for flows of mild intensity one can assume that the static structure is only slightly distorted by the flow. In this case, the correction due to collective diffusion can be applied by using the equilibrium theory of liquids. Hence, the stationary Smoluchowski equation with convection can be written as

$$-\frac{1}{b}\nabla \cdot \left[\frac{\partial \Pi}{\partial \rho}\nabla \rho + (-\nabla U + b\mathbf{v})\rho\right] = 0 \qquad (20)$$

where **v** is the macroscopic velocity field.[8,29] The types of flows that are encountered in the physical world invariably have an anisotropic geometry.[28] Hence, the one above is a partial differential equation in the spherical coordinates frame centered on a moving particle (i.e., the sink, for our purpose). As shown in recent work,[30] the problem can be reduced to a spherically symmetric one for the determination of the aggregation/reaction rates, since the net flux is an integral quantity over the control spherical volume around the moving particle

$$\kappa = 4\pi r^2 D\left[\left(\frac{\partial \Pi}{\partial \rho}\frac{\partial \langle\rho\rangle}{\partial r} + \beta\,\frac{\partial U}{\partial r}\langle\rho\rangle\right)\right] + 4\pi r^2 kT\langle v_r^+ \rho\rangle \quad (21)$$

where $\langle...\rangle$ indicates the angular average in spherical coordinates. v_r^+ denotes the positive part of the radial component, v_r, of the fluid velocity **v**. This is responsible for the nonvanishing contribution to the inward particle flux and is defined by[30]

$$v_r^+(\mathbf{r}) = \max(v_r(\mathbf{r}), 0) = \begin{cases} v_r(\mathbf{r}) & \text{if } v_r(\mathbf{r}) > 0 \\ 0 & \text{else} \end{cases}$$

For flows of mild intensity, we can assume $\langle v_r^+(\mathbf{r})\,\rho(\mathbf{r})\rangle \approx \langle v_r^+(\mathbf{r})\rangle\langle\rho(\mathbf{r})\rangle$; i.e., the flow field and the particle-density field are weakly coupled. Hence, we arrive at the following effective Smoluchowski equation in the orientation-averaged particle-density field[30]

$$\frac{(b^{-1})}{r^2}\frac{d}{dr}\left[r^2\left(\beta\frac{dU}{dr} + b\langle v_r^+\rangle\right)\langle\rho\rangle + r^2\frac{\partial\Pi}{\partial\rho}\frac{d\langle\rho\rangle}{dr}\right] = 0 \quad (22)$$

In the important case of linear flows, this simplified equation still presents significant mathematical complexity, due to the singularity induced by the term v_r^+ at $r = \infty$, i.e., at the location of the far-field boundary condition. The Smoluchowkski equation with shear is indeed a well-known singularly perturbed equation with an inner boundary layer of thickness δ along the r axis, within which both diffusion and convection are important, and an outer layer, where convection is predominant.[31] The reaction rate is clearly determined by the solution in the inner layer, which can be found by integrating the equation within the inner boundary layer.[30] The solution for the reaction rate is thus given by[30]

$$\frac{\kappa}{\kappa_S} = \frac{\beta\Pi(\rho_\infty)}{\rho_\infty}\left[2\int_0^\delta d\xi\frac{\exp\left[\int_\delta^\xi ds(\beta\,dU_{\text{eff}}/ds + Pe\langle\tilde{v}_r^+\rangle)\right]}{G(\xi)(\xi+2)^2}\right]^{-1}$$
$$(23)$$

where $\xi = (r - R)/R$, with the contact radius $R = R_s + R_p$, and $G(\xi)$ is the hydrodynamic function accounting for viscous retardation (which are always important in the presence of flow). As shown in ref 30, the boundary-layer thickness can be estimated as $\delta \approx R_p[(\lambda/R_p)/Pe]^{1/2}$, where λ (a surface-to-surface distance) is the decay length of the effective interaction and Pe is the Peclet number. $\tilde{v}_r^+ = v_r^+/(\dot\gamma R_p)$ has been made dimensionless by dividing by the shear-rate $\dot\gamma$ multiplied by the particle radius. Further hydrodynamic interactions can be accounted for at two-body level through the expression of $\tilde{v}_r^+$, which for the case of simple shear reads $\tilde{v}_r^+ = -(1/3\pi)(\xi+2)\cdot[1 - A(\xi)]$. The hydrodynamic function $A(\xi)$ can be given in
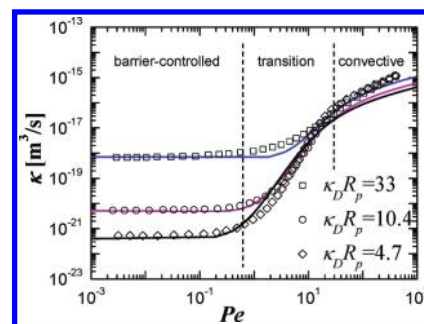
Figure 9. Theoretical curves for the reaction rate in the dilute limit in the presence of an intermolecular (DLVO) potential and shear flow upon varying the value of the Debye screening parameter and for equal-sized colloidal particles, $R_p = 100$ nm and $\psi_0 = -0.015$ V. The symbols are the numerical solution of the full eq 20 according to ref 33.

analytical form for simple shear and other elementary linear flows.[26,32] Predictions from eq 23 for the kinetic constant of aggregation of DLVO-interacting colloidal particles in the *dilute* limit are in good quantitative agreement, without any adjustable parameters, with the full numerical solution of the partial differential equation (eq 20) in the dilute case ($d\Pi/d\rho = 1$), as shown in Figure 9.

The flat plateau at low Peclet numbers (i.e., at low shear rates) corresponds to a regime where the encounter kinetics is still completely dominated by the reaction barrier and the effect of flow is insignificant (barrier-controlled regime in the picture). The effect of the flow on the rate becomes significant as the boundary-layer (whose thickness decreases with increasing Pe) becomes comparable with the range of the reaction barrier. Then the flow field enhances the barrier-hopping process and therefore effectively speeds up the encounter kinetics. Upon further increasing the Peclet number, there is a rapid increase in the rate until the boundary-layer becomes so thin that the kinetics is dominated by the convective transport rate (convective regime in the picture).[30]

Equation 23 can be used to estimate the reaction kinetics when the system of Figure 1 is subjected to a macroscopic shear flow. The most general case is when the effects of electrostatics, crowding, and flow are simultaneously present. This can be described by eq 23 by setting $U_{\text{eff}} = U^{\text{DLVO}} + U_2^{(s)}$.

Equation 23 can be reduced to an explicit form in the regime where the kinetics is dominated by a sharp barrier. This is possible if one does a steepest-descents approximation of the inner integral in eq 23. We start by noting that

$$\int_0^\delta d\xi\frac{\exp\left[\int_\delta^\xi ds(\beta\,dU_{\text{eff}}/ds + Pe\langle v_r^+\rangle)\right]}{G(\xi+2)^2}$$
$$\approx \int_0^\delta d\xi\frac{\exp\left[\beta U_{\text{eff}} - Pe(\xi+2)^2/2\right]}{G(\xi+2)^2} \quad (24)$$

where for simplicity we have neglected the hydrodynamic interactions in the velocity term. Indeed, if U_{eff} features a prominent absolute maximum, so does also the whole function in the argument of the exponential, which can be expanded to second order around the point of maximum. In this way the integral on the rhs of eq 24 becomes Gaussian and we finally

obtain

$$\frac{\kappa}{\kappa_S} \approx \sqrt{\frac{1}{3\pi}Pe - \beta U''_{\text{eff,m}}} \exp(-\beta U_{\text{eff,m}} + 2Pe/3\pi) \quad (25)$$

where $U_{\text{eff,m}}$ is approximately equal to the value of the effective potential at the maximum. This approximation holds only when there is a prominent absolute maximum in the function $\beta U_{\text{eff,m}} + 2Pe/3\pi$. If we consider the case $U_{\text{eff}} = U_2^{(s)}$ (with $U_2^{(s)}$ given by eq 5 and Figure 2a), where the crowding is the only effective potential barrier for the convective-diffusive transport, we get

$$\frac{\kappa}{\kappa_S} \propto \exp[-cZ(\rho_\Delta) + 2Pe/3\pi] = \exp[-cZ(\rho_\Delta) + 2\mu\dot{\gamma}R_p^3/kT]$$

$$(26)$$

Equation 26, in a very compact fashion, suggests that the effective barrier due to the crowding alone can be lowered by the flow, i.e., whenever $\dot{\gamma} > 0$. Hence, if it is true that the crowding represents an additional resistance to the diffusive transport, it seems also true that the presence of convection can effectively reduce this resistance. The solution to eq 23 with crowding and electrostatics is going to bring new insights into this mechanism, as will be shown in the next section. The low-Peclet plateau corresponds to a regime where the kinetics is controlled by the barrier and aggregation/reaction occurs with an activation delay. In correspondence of a critical Peclet value, the argument of the exponential in the outer integral of eq 23 vanishes, which causes the activation barrier and the delay in the kinetics to vanish as well. Hence, the rate transitions to a fast regime controlled by the shear, where in fact the kinetics goes roughly with the cube of the shear rate, as predicted by the theory of shear-induced aggregation (originally due to Smoluchowski[28,34]). From a physical viewpoint, the shear helps the incoming particle in crossing the barrier due to the crowding (and to the adverse osmotic pressure gradient) around the reactant, thus effectively decreasing the barrier. At some value of the Peclet, the shear force becomes equal to the repulsive force due to the crowding, so that the net barrier vanishes. Upon further increasing the shear rate, the transport is completely controlled by convection and the kinetics thus follows the mechanism of purely shear-induced aggregation.

This is the picture that emerges from a very approximate analysis. In the following section we are going to see how a nontrivial and surprising effect, hidden in the boundary-layer structure of the full eq 23, arises from the interplay between shear and crowding.

B. Results and Discussion. The encounter rate for conditions of crowding corresponding to $\phi = 0.40$ and $R_s/R_p = 1/30$ in shear flow is plotted as a function of the Peclet number for the case of DLVO intermolecular interactions between particles $R_p = 30$ nm and sink $R_s = 1$ nm in Figure 10. The parameters of the effective (DLVO + crowding) potential are the same as for the curves in Figure 7 and correspond to the set of conditions 5–8 in Table 1. Further, many-body hydrodynamic interactions, which are very important in flowing systems, have been accounted for at the level of effective-medium theory by replacing the solvent viscosity with the (hard sphere) suspension viscosity.[8] This amounts to taking an effective diffusion coefficient $D(\phi) = M(\phi)\, d\Pi(\phi)/d\phi$ with an effective mobility given by $M(\phi) = b^{-1}[\eta(\phi)/\mu]^{-1}$, where $\eta(\phi)$ is the effective viscosity of the suspension, while μ is the viscosity of the pure solvent. For $\eta(\phi)$ we use the equation recently proposed by Mendoza and Santamaria-Holek.[35]
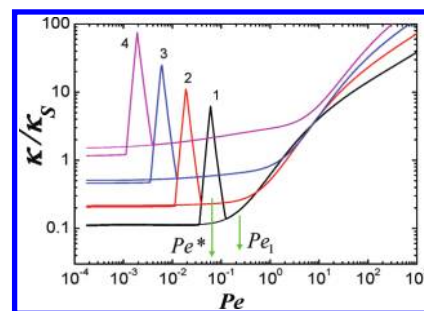
Figure 10. Theoretical curves for the encounter rate in the presence of an effective potential (crowding + DLVO) and shear flow. Dotted lines: $U_{\text{eff}} = U^{\text{DLVO}}$. Solid lines: $U_{\text{eff}} = U^{\text{DLVO}} + U_2^{(s)}$. (1) $I = 1$ mM, (2) $I = 10$ mM, (3) $I = 100$ mM, and (4) $I = 1000$ mM. $R_p = 30$ nm and $R_s = 1$ nm $\psi_0 = -0.020$ V.

For comparison, the curves corresponding to the dilute limit are plotted as dotted lines. It is seen that all the curves that take crowding into account feature a narrow, edge-shaped bump of nearly 2 order of magnitude in the encounter rate at low Peclet numbers. This unexpected feature can be explained by considering the interplay between the convective–diffusive boundary-layer and the effective potential with crowding. According to the theory of ref 30, the thickness of the boundary layer is given by $\delta = R_p[(\lambda/R_p)/Pe]^{1/2}$. Hence, upon increasing the Peclet number, δ decreases and eventually becomes equal to the radial position of the crowding barrier. We denote the value of Peclet at which this occurs as Pe^*. When $Pe = Pe^*$ the incoming particle that is injected into the boundary layer from the convective flow finds itself in an activated state, depicted schematically in Figure 11a.

Thanks to this activated-state, the incoming particle is greatly facilitated in jumping over the electrostatic interaction barrier and this results in a greatly enhanced encounter rate. On the other hand, for values of Peclet that are larger than Pe^*, such as $Pe_1 > Pe^*$, the situation is exactly the same as for the infinitely dilute system with no crowding, since the particle is injected by the convective flow into a boundary layer that is thinner than the crowding barrier, as shown schematically in Figure 11b. Therefore, the effect of crowding plays no role in this regime, so there is no difference between dilute and crowded conditions. From a slightly different perspective, this happens because at sufficiently high Peclet the radial position of the crowding barrier falls into the outer purely convective layer, where convection dominates over any other kind of interaction. According to our theory, the value of Peclet at which this bump occurs can be estimated using the relation

$$R_p\sqrt{(\kappa_D R_p)^{-1}/Pe^*} = R_p + \Delta = (5/3)R_p \quad (27)$$

from which one gets

$$Pe^* = \left(\frac{10}{3}\frac{R_p}{R}\right)^2 \frac{2}{\kappa_D R} \quad (28)$$

This is a highly nontrivial effect due to the interplay between crowding and shear, as one would expect that the crowding merely acts as to lower the encounter rates. The boundary-layer structure of the Smoluchowski equation with shear,[31] instead, as we have seen, gives rise to a peculiar activated-state when the boundary-layer thickness is equal to the location of the crowding barrier. From this activated-state the incoming Brownian particle can jump, over the electrostatic barrier, directly into the absorbing boundary.
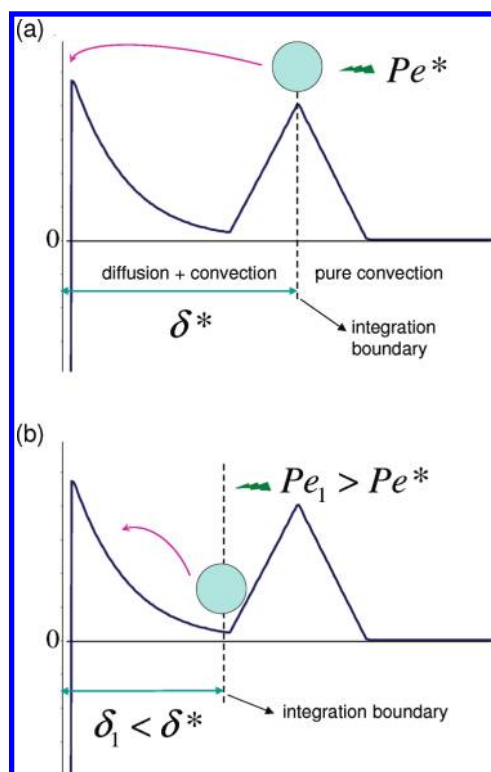
Figure 11. (a) Schematic depiction of the activated-state that arises when the Peclet-dependent boundary-layer thickness is equal to the location of the crowding barrier. (b) Upon further increasing the Peclet above Pe^*, there is no effect of crowding as the crowding barrier falls in the convective outer layer, which is completely controlled by convection, which overwhelms any finite barrier. $\delta_1 = R_p[(\lambda/R_p)/Pe_1]^{1/2}$, also with reference to Figure 10.

Although in the above figures also predictions from the present theory for fairly high Peclet numbers have been present, a caveat is necessary. Indeed, the present theory treats the effective potential due to crowding as if it was isotropic, i.e., as spherically symmetric around the reactant. At high Peclet numbers, this is certainly not true, since there the intense shear field breaks the spherical symmetry in the radial distribution function and the distribution of particles in the first coordination shell is *anisotropic*.[31] It is not at all obvious how this symmetry breaking due to shear will affect the kinetic constant. This information is very difficult to obtain by the means of theory alone and dedicated simulations will be necessary in the future to clarify this point.

C. Remarks on the Effect of Many-Body Hydrodynamic Interactions. A final note concerns many-body hydrodynamics. Clearly, in real systems at high concentrations and with shear flow, many-body hydrodynamic interactions play a significant role. Even though there is no way to incorporate them into the analysis, which is at the same time simple and accurate, we must content ourselves with a rough estimate of many-body HI within our theory by using an effective medium approach.[31] The final result can also be derived using a "mode coupling" method as shown in ref 36. Within this approach, as mentioned in the previous section, one assumes an effective volume-fraction-dependent diffusion coefficient $D(\phi)$, where the viscosity of the solvent μ is replaced by the viscosity of the medium η

$$D(\phi) = [b(\phi)]^{-1}\, d\Pi(\phi)/d\phi \qquad (29)$$

where

$$b(\phi) = 6\pi\eta(\phi)R_p \qquad (30)$$

leading to

$$\kappa/\kappa_S = [\eta(\phi)/\mu]^{-1}\beta Z(\phi)\left(R\int_R^\infty \frac{e^{\beta U_2^{(s)}}}{r^2}\, dr\right)^{-1} \qquad (31)$$

Let us consider the effect of many-body HI on the reaction kinetics without shear flow and without intermolecular interactions. It is reasonable to expect that many-body HI lead a significant slow-down in the kinetics in addition to the effect of the crowding. Further, we notice that in the presence of HI the maximum in the rate caused by crowding (that was explained and analyzed in detail in section III) may get shifted to significantly lower ϕ. Hence we conclude that many-body HI may greatly enhance the effect of crowding. This becomes evident also considering that $d[1/b(\phi)]/d\phi < 0$. This additional dependence on ϕ can "accelerate" the onset of the slowing-down with increasing ϕ caused by the crowding barrier (cf. section II). We believe that dedicated simulation studies accounting for the hydrodynamics can, in the future, shed more light on this aspect.

IV. CONCLUSION

In this paper, we present an analytical theory for the diffusive reaction rate of chemical reactions under crowding and shear conditions. In particular, we have shown how the celebrated Smoluchowski rate is modified in this case. Crowding is implemented as an effective potential induced by the structuration of the solvent, an approach that has been shown to be in quantitative agreement with the results of computer simulations.[21] On the other hand, shear has been introduced by modifying the Smoluchowski equation to include convection; see eq 20. This method has been recently introduced to describe the effect of aggregation experiments.[37] Here we have unified the two approaches to discuss the concurrent effects of crowding and shear. In order to present a stronger link with experiments, we have discussed the case of a colloidal and of a nanoparticle system both interacting by a DLVO potential. These two cases already show a different behavior when the shear is not present. Due to the different length scales involved in the process, the colloidal system reaction rate is not heavily affected by crowding as long as the DLVO potential is present, i.e., until the reaction becomes diffusion limited. For the nanoparticle, however, crowding seems to always slow down the reaction in both reaction and diffusion-limited regime.

One of the main findings of this work, however, concerns the case in which the DLVO nanoparticle is simultaneously under shear and crowding conditions. In this case there exists a critical Peclet number, i.e., Pe^*, at which the reaction rate is increased by orders of magnitude; see Figure 10. This happens when the shear takes on the right magnitude to overcome the crowding barrier and to inject the reactant particle exactly on top of it, creating a sort of activated state. When the particle is injected by the flow into the boundary layer at this special distance, it is in a highly crowded environment, as can be seen by the form of the density profiles.[21] As a consequence of this environment, the particle gains a further osmotic *drive* that enhances the probability of passing through the electrostatic (DLVO) barrier; see the cartoon in Figure 11. This seems to suggest that there is a

possible way of coupling crowding-induced density fluctuations with the shear in order to increase the reaction rate. For higher Pe, the particle is not injected in the coordination shell but rather between the two maxima of the effective potential. This means that the particle is in between the sink and the high-density region and does not gain any osmotic pressure; see the cartoon in Figure 11.

The theory presented here is very idealized, but we believe it contains the right ingredients. In particular, it highlights the direction to follow for future investigations. For a proper description of crowding, the next step would be a theory capable of predicting the density profiles and effective potentials in a self-consistent way. To this aim a promising direction seems to be dynamical density functional theory (DDFT), for which several functional forms for the free energy have been discussed (for a recent review see, for example, ref 38). For what concerns shear, the assumption that the density profile does not get distorted under shear is reasonable only for small Pe. At higher shear rate a way of coupling shear and density distribution would be of great importance. It must be stressed, however, that the enhancement in the reaction rate, described here, occurs for low Peclet numbers, where the cage around the sink is probably not seriously distorted. A more general theory should take distortion of the density into account. In this sense, recent ideas from mode-coupling theory under shear could be inspirational.[39]

The most reliable way to test some of the theoretical predictions presented here is probably to perform systematic, physical and computational, experiments. In this sense, an especially interesting set of experiments would be one where the time scale of aggregation of dense (e.g., $\phi = 0.5$) colloidal systems under shear is measured over a broad range of shear rates/Peclet. The theory with no account of crowding effects[30,37] predicts that the characteristic time scale $\tau \sim \kappa^{-1}$ is an exponential *monotonically* decreasing function of the Peclet number. On the other hand, the full theoretical model accounting for the effect of crowding (eq 23) that has been proposed here predicts a departure from the exponential law occurring in a limited range of Peclet with a local minimum in $\tau = f(Pe)$. Experimentally, the aggregation time scale could be assessed either microscopically, e.g., using scattering techniques to measure doublet-formation rates,[40] or macroscopically, from the sudden upturn of the viscosity at the onset of aggregation.[37] In both cases, it would be essential to design experimental systems where colloidal stabilization is such to guarantee measurable aggregation time scales under shear. An alternative experimental setup could be one where a certain number of sinks (for example, particles coated with some receptors, like streptavidin) is immersed in a sea of background particles that do not interact with each other but are selectively bounded by the sink particles.

Another direction where the model has to be refined, in order to make it applicable to cellular environments, has to do with the spherical and isotropic assumption of the particles. It is clear that macromolecular species in the cells are far from being spherical and may exhibit anisotropic ("patchy") interactions. A first step along this direction is the understanding of the dynamics and phase behavior of nonspherical and patchy particle systems.[47,48]

At the end of the paper, we have shown that within a simple, effective medium approach the effect of hydrodynamic interactions can be very important. This is a point that deserves further investigation and we hope that the present paper will stimulate new numerical and theoretical investigations on the subject. Another important aspect to investigate would be the effect of attraction on the reaction rates. It has been shown, for example,

that a compensation between enthalpy and crowding can lead to equilibrium association constants.[41]

Concluding, we believe that the interplay between crowding and shear in reaction kinetics can play an important role in colloidal science, biology, and nanomaterials. It could suggest new routes to control the rates and to understand the behavior of living matter where crowding is more the rule than an exception.

■ APPENDIX: FROM THE SMOLUCHOWSKI EQUATION TO KINETIC RATES

The probability distribution for a free Brownian particle of mass m in space and time in one dimension $p(x,v,t)$ is governed by the Fokker–Planck equation[8]

$$\frac{\partial p}{\partial t} = -\mathbf{v} \cdot \nabla p + \frac{b}{m} \nabla_{\mathbf{v}} \cdot \left(\mathbf{v} p + \frac{kT}{m} \nabla_{\mathbf{v}} p \right) \qquad (32)$$

$b = 6\pi\mu R_p$ is the viscous friction coefficient under stick boundary conditions for an isolated particle in a liquid, with μ being the viscosity of the liquid and R_p the hydrodynamic particle radius. This is equivalent to a Langevin equation for position and velocity given by $m(d\mathbf{v}/dt) = -b\mathbf{v} + \mathbf{X}(t)$, where $\mathbf{X}(t)$ represents the fluctuating force.[7] Under the influence of external forces or interparticle potentials, the latter becomes[7,8]

$$m\frac{d\mathbf{v}}{dt} = -b\mathbf{v} + \mathbf{X}(t) + \mathbf{K}(\mathbf{x}) \qquad (33)$$

where $\mathbf{K}(\mathbf{x})$ is the resultant of these forces. From the solution to the Langevin equation it can be shown that the velocity reaches a steady state $(d\mathbf{v}/dt \rightarrow 0)$ after a transient that goes as $\sim\exp(-bt/m)$. Hence for large b/m the velocity relaxes exponentially fast to its stationary value. In other words, the changes in the particle velocity can be observed only on a time scale that is extremely short. As an example we consider a particle of polystyrene in water with a diameter of 10 μm. For such a particle, even though its size is already close to the upper limit of the "colloidal domain", one calculates $b/m \simeq 1.71 \times 10^8$ s^{-1} so that the transient (where the momentum is not yet relaxed to equilibrium) is on the order of 10^{-8} s. It is evident that for all processes occurring on larger time scales, the momentum of our particle can be safely assumed in equilibrium. On the other hand, for particles of denser material in a gaseous phase, including ionized gases, as is the case of dusty plasmas in microgravity, where μ is very small (on the order of μPa s) and the particle inertia much larger, the ratio b/m has typically much smaller values $(10^{-3}-10^{-4}$ s$^{-1})$, thus making the assumption of the equilibration of momentum invalid. In this case, one has to resort to the full Fokker–Planck equation in both coordinate and momentum space.[42,43] The steady-state velocity can be evaluated from eq 33 by imposing $d\mathbf{v}/dt = 0$ and the Langevin equation becomes $dx/dt = b^{-1}[\mathbf{X}(t) + \mathbf{K}(\mathbf{x})]$. The latter can be shown[7] to be equivalent to the following Fokker–Planck equation

$$\frac{\partial \rho}{\partial t} = \frac{1}{b} [\nabla \cdot (-\mathbf{K}(\mathbf{x})\rho + kT\nabla\rho)] \qquad (34)$$

where $\rho = \int p(\mathbf{x},\mathbf{v},t) \, d^3v$. Equation 34 is the one-dimensional Smoluchowski equation. A rigorous derivation involves much formalism and can be found e.g. in.[44] What is important to notice is that the limit of large friction b/m implies short relaxation times for the particle velocity $\mathbf{v}$, which thus relaxes to its stationary value within a time interval during which $x =$ const.[8] This is what leads to the so-called adiabatic elimination of the fast variable $\mathbf{v}$
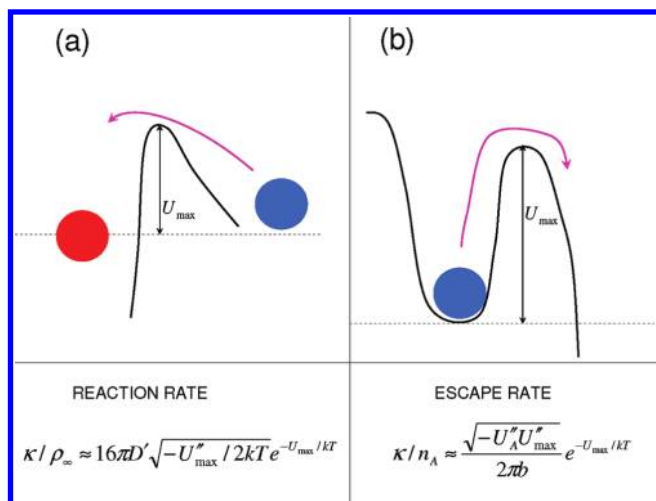
Figure 12. Schematic of the physical situations to which eqs 41 and 48 apply, respectively.

and makes the use of eq 34 feasible in the overdamped limit, i.e., whenever b/m is large.[8] By taking the macroscopic limit, $\rho \rightarrow c$ where c is the number of particles per unit volume, eq 34 is seen to be identical to the diffusion equation in a field of forces.[45] Further, eq 34 can be generalized to a system of N particles

$$\frac{\partial}{\partial t}\rho(\mathbf{x}_1...\mathbf{x}_N, t) = \mathscr{L}_S \rho(\mathbf{x}_1...\mathbf{x}_N, t) \tag{35}$$

with the many-particle Smoluchowski operator (neglecting hydrodynamic interactions) defined by

$$\mathscr{L}_S(...) = D_0 \sum_{j=1}^{N} \nabla_{x_i} \cdot \{\beta[\nabla_{x_j}U](...) + \nabla_{x_j}(...)\} \tag{36}$$

where $\mathbf{x}_1...\mathbf{x}_N$ is the set of coordinates of the N particles and $\beta = 1/kT$.[8] This equation is the starting point for dynamical density functional theory approaches to the modeling of colloidal suspensions[10,11] which allow one to account for hydrodynamic interactions between the Brownian particles. It is also the starting point for mode-coupling theory approaches for dense suspensions in the glassy regime.[39] In this work we will focus our analysis on the treatment of simultaneously present many-particle interaction and external-field effects within the one-dimensional formalism by making use of effective potentials.

In order to estimate the time scale of physical processes, one is generally interested in the stationary value of the probability distribution.[45] The stationary behavior is obtained by setting $\partial\rho/\partial t = 0$ in eq 34. Assuming spherical symmetry, the latter can be integrated once to give the flow rate of particles onto the spherical surface

$$\kappa = \frac{4\pi r^2}{b}\left(-K(r)\rho + kT\frac{\partial\rho}{\partial r}\right) = \text{const} \tag{37}$$

where r is the radial distance between the particles. If the external forces are conservative, $K(r) = -\partial U(r)/\partial r$, we have that the current can be written as

$$\kappa = \frac{4\pi kT[\rho e^{U/kT}]_B^A}{\int_A^B \frac{b}{r^2}e^{U/kT}\,dr} \tag{38}$$

upon integration between two points A and B. The general steady-state solution to the one-dimensional Smoluchowski equation with a conservative potential is[13,14]

$$\rho = Ce^{-U/kT} - (\kappa/8\pi)e^{-U/kT}\int \frac{1}{r^2}\frac{b}{kT}e^{U/kT}\,dr \tag{39}$$

where κ is given by eq 38 and C is an integration constant. A few simple cases can be described straightaway by making use of eq 39. Let us first consider the case where U is an electrostatic potential, such that $U = 0$ at $r = A = \infty$ (r is the radial coordinate in a spherical geometry) and there is an absorbing boundary at $r = B = 2R_p$ such that $\rho(B) = 0$. This represents the case of diffusion of charged Brownian particles toward a reference particle (placed at the center of a spherical coordinates frame) under the stick-upon-contact condition. The situation is schematically depicted in Figure 12a. Replacing these conditions in eq 39 leads to the well-known result for the reaction rate[14,15]

$$\kappa = \frac{4\pi D'\rho_\infty}{\int_0^\infty \frac{1}{r^2}e^{U/kT}\,dr} \tag{40}$$

where $\rho_\infty = \rho(r = \infty)$ and $D' = 2D = 2kT/b$ accounts for the fact that the diffusion of two particles against each other is accelerated by a factor of 2 with respect to self-diffusion. $r = 0$ is taken as the absorbing boundary, i.e., as the coordinate where the surface-to-surface distance between the particles is zero. Equation 39 can be used to give the aggregation rate between colloidal particles interacting with an effective interaction potential given by the DLVO theory (i.e., a superposition of van der Waals attraction and screened electrostatic repulsion).[24,14] If the latter, as is true in most cases, comprises a repulsive barrier, the integral in the denominator can be simplified by the steepest descent method, since the main contribution comes from near the barrier top.[25] Hence we write $U \approx U_{max} + (1/2)U_{max}''(r - r_{max})^2$. One should note that $U_{max}'' < 0$. The integral is now Gaussian, which gives[25]

$$\kappa \approx 16\pi D'\rho_\infty\sqrt{-U_{max}''/2kT}\,e^{-U_{max}/kT} \tag{41}$$

In the case of $U = 0$ everywhere, eq 39 reduces to the well-known diffusion-limited reaction (aggregation) rate due to Smoluchowski[34]

$$\kappa_S = 4\pi RD'\rho_\infty \tag{42}$$

where $R = 2R_p$ is the encounter distance (coagulation radius). Furthermore, one-dimensional Smoluchowski equations, i.e.

$$\frac{\partial\rho}{\partial t} = \frac{1}{b}\left[\frac{\partial}{\partial x}\left(-F(x)\rho + kT\frac{\partial\rho}{\partial x}\right)\right]$$

can be used to estimate the rate of escape of a Brownian particle from a deep metastable potential well-centered in $x = A$.[13] This situation is schematically depicted in Figure 12b. For simplicity, we will consider a one-dimensional space with coordinate x. We define the rate as κ/n_A with

$$n_A = \int_{-\infty}^{+\infty}\rho(x)\,dx \tag{43}$$

Within the potential well we can write

$$\rho(x) \approx \rho_A\exp(-\beta[U(x) - U(A)]) \tag{44}$$

with $U(x) \approx U_A + 1/2U_A''(x - x_A)^2$. Upon replacing in eq 43

7394

dx.doi.org/10.1021/jp200439a | *J. Phys. Chem. B* 2011, 115, 7383–7396

we get

$$n_A = \rho_A \sqrt{\frac{2\pi kT}{U_A''}} \tag{45}$$

The rate at which a particle originally trapped at A escapes to B is expressed by the ratio

$$\frac{\kappa}{n_A} = \frac{1}{b} \sqrt{\frac{U_A'' kT}{2\pi}} \left(\int_A^B e^{U/kT} \, dx \right)^{-1} \tag{46}$$

Also the remaining integral can be reduced to Gaussian by using the saddle-point approximation (the main contribution to the integral comes from the top of the barrier): $U \approx U_{max} + (1/2) U_{max}''(x - x_{max})^2$, giving

$$\int_A^B e^{U/kT} \, dx = e^{U_{max}/kT}$$

$$\int_{-\infty}^{+\infty} \exp[U_{max}''(x - x_{max})^2/2kT] \, dx = \sqrt{\frac{2\pi kT}{-U_{max}''}} e^{U_{max}/kT} \tag{47}$$

The Kramers escape rate is thus given by[13]

$$\kappa/n_A = \frac{\sqrt{-U_A'' U_{max}''}}{2\pi b} e^{-U_{max}/kT} \tag{48}$$

It is interesting to compare eqs 41 and 48 and the two situations that they describe, shown in panels a and b of Figure 12, respectively. Apart from numerical prefactors related to geometry (spherical-isotropic versus 1D), both equations are in Arrhenius form, with an exponential term in the activation barrier and a pre-exponential term giving the frequency of particles coming to the barrier. Both rates are dominated by the exponential term in the barrier height, which reflects the controlling physical phenomenon (i.e., the thermally activated barrier-hopping). However, the two situations differ in the "injection point". In the case of eq 41, see Figure 12a, the particles are "injected" directly from the bulk of the system (e.g., a colloidal suspension) where $\rho = \rho_\infty$. In the other case of eq 48, see Figure 12b, the particles are injected from the metastable well at A, where thermal equilibrium has been practically established due to the steepness of the energy landscape. The differences in the local landscape of the injection point (flat for eq 41 and a well in the case of eq 48) clearly do not affect the exponential activation term but result in different frequency prefactors. Although they are both inversely proportional to the friction b and to $(-U_{max}'')^{1/2}$, in the first case there is an additional proportionality to $\rho = \rho_\infty$, while in the Kramers escape rate the additional proportionality is to $(U_A'')^{1/2}$. These differences are expected to vanish in the limit of very large U_{max}, where the rates are completely dominated by the exponential term. The most interesting physics in soft condensed matter occurs in out-of-equilibrium situations, where the system evolves through a series of structural transformations. Such transformations usually involve either aggregation (structure-formation) or breakdown processes. In particular, eqs 41 and 42 represent the archetypical form of an aggregation process (where the injection from the bulk represents the initial conditions of a disperse system), while eq 48 provides the basis to describe yielding/melting processes (where the injection point is a bound state).[46]

■ AUTHOR INFORMATION

Corresponding Author
*E-mail: alessio.zaccone@chem.ethz.ch; az302@cam.ac.uk.

■ REFERENCES

(1) de Gennes, P. G. *Rev. Mod. Phys.* **1992**, *64*, 645–648.
(2) Likos, C. N. *Phys. Rep.* **2001**, *348*, 267–439.
(3) Frenkel, D. *Science* **2002**, *296*, 65–66.
(4) Ottinger, H. C. *MRS Bull.* **2007**, *32*, 936–940.
(5) Einstein, A. *Ann. Phys.* **1905**, *17*, 549–560.
(6) von Smoluchowski, M. *Ann. Phys.* **1905**, *21*, 756–780.
(7) Uhlenbeck, G. E.; Ornstein, L. S. *Phys. Rev.* **1930**, *36*, 823–841.
(8) Dhont, J. *An Introduction to the Dynamics of Colloids*; Elsevier: Amsterdam, The Netherlands, 1996.
(9) deGennes, P. G. *J. Chem. Phys.* **1974**, *60*, 5030–5042.
(10) Archer, A. J.; Evans, R. *J. Chem. Phys.* **2004**, *121*, 4246–4254.
(11) Rex, M.; Loewen, H. *Phys. Rev. Lett.* **2008**, *101*, 148302.
(12) Risken, H. *The Fokker−Planck Equation*; Springer: Berlin, 1999.
(13) Kramers, H. A. *Physica* **1940**, *7*, 284–304.
(14) Verwey, E. J. W.; Overbeek, J. Th. G. *Theory of the Stability of Lyophobic Colloids*; Elsevier: New York, 1948.
(15) Ovchinnikov, A. A.; Timashev, S. F.; Belyi, A. A. *Kinetics of Diffusion Controlled Chemical Processes*; Nova Science Publishers: New York, 1989.
(16) Dzubiella, J.; McCammon, J. A. *J. Chem. Phys.* **2005**, *122*, 184902.
(17) Hansen, J. P.; McDonald, I. R. *Theory of Simple Liquids*; Academic Press: New York, 1986.
(18) Hall, K. R. *J. Chem. Phys.* **1972**, *57*, 2252–2254.
(19) De Michele, C. *J. Comput. Phys.* **2010**, *229*, 3276–3294.
(20) Scala, A.; De Michele, C.; Voigtmann, T. *J. Chem. Phys.* **2007**, *126*, 134109.
(21) Dorsaz, N.; De Michele, C.; Piazza, F.; De Los Rios, P.; Foffi, G. *Phys. Rev. Lett.* **2010**, *105*, 120601.
(22) Dijkstra, M.; van Roij, R.; Evans, R. *Phys. Rev. E* **1999**, *59*, 5744.
(23) Kirkwood, J. G. *J. Phys. Chem.* **1957**, *43*, 97–107.
(24) Derjaguin, B. V.; Landau, L. D. *Acta Physicochim. USSR* **1941**, *14*, 633–652.
(25) Derjaguin, B. V. *Theory of Stability of Colloids and Thin Films*; Plenum Press: Consultants Bureau: New York, 1989.
(26) Russel, W. B.; Saville, D. A.; Schowalter, W. R. *Colloidal Dispersions*; Cambridge University Press: Cambridge, 2001.
(27) Holm, C.; Kekicheff, P.; Podgornik, R. (Eds.) *Electrostatic Effects in Soft Matter and Biophysics*; Kluwer Academic: Dordrecht, 2000.
(28) Levich, V. G. *Physicochemical Hydrodynamics*; Prentice-Hall: Englewood Cliffs, NJ, 1962.
(29) Doi, M.; Edwards, S. F. *The Theory of Polymer Dynamics*; Oxford University Press: Oxford, 1986.
(30) Zaccone, A.; Wu, H.; Gentili, D.; Morbidelli, M. *Phys. Rev. E* **2009**, *80*, 051404.
(31) Dhont, J. K. G. *J. Fluid Mech.* **1989**, *204*, 421431.
(32) Batchelor, G. K.; Green, J. T. *J. Fluid Mech.* **1972**, *56*, 375–400.
(33) Melis, S.; Verduyn, M.; Storti, G.; Morbidelli, M. *AIChE J.* **1999**, *45*, 1383–1393.

7395

dx.doi.org/10.1021/jp200439a |*J. Phys. Chem. B* 2011, 115, 7383–7396

(34) von Smoluchowski, M. *Z. Phys. Chem.* **1917**, *92*, 129.

(35) Mendoza, C. I.; Santamaría-Holek, I. *J. Chem. Phys.* **2009**, *130*, 044904.

(36) Kholodenko, A. L.; Douglas, J. F. *Phys. Rev. E* **1995**, *51*, 1081–1090.

(37) Zaccone, A.; Gentili, D.; Wu, H.; Morbidelli, M. *J. Chem. Phys.* **2010**, *132*, 134903.

(38) Roth, R. *J. Phys.: Condens. Matter.* **2010**, *22*, 063102.

(39) Fuchs, M.; Cates, M. E. *J. Rheol.* **2009**, *53*, 957–1000.

(40) Schneider, C.; Jusufi, A.; Farina, R.; Pincus, P.; Tirrell, M.; Ballauff, M. *Phys. Rev. E* **2010**, *82*, 011401.

(41) Douglas, J. F. *Phys. Rev. Lett.* **2009**, *103*, 135701.

(42) Shukla, P. K.; Mamun, A. A. *Introduction to Dusty Plasma Physics*; IOP: Bristol, 2001.

(43) Dorsaz, N.; De Michele, C.; Piazza, F.; Foffi, G. *J. Phys.: Condens. Matter* **2010**, *22*, 104116.

(44) Stratonovich, R. L. *Topics in the Theory of Random Noise*; Gordon and Breach: New York, 1967.

(45) Lifshitz, E. M.; Pitaevskii, L. P. *Physical Kinetics*; Butterworth-Heinemann: London, 1981.

(46) Smith, P. A.; Petekidis, G.; Egelhaaf, S. U.; Poon, W. C. K. *Phys. Rev. E* **2007**, *76*, 041402.

(47) De Michele, C.; Schilling, R.; Sciortino, F. *Phys. Rev. Lett.* **2007**, *98*, 965702.

(48) Corezzi, S.; De Michele, C.; Zaccarelli, E.; Fioretto, D.; Sciortino, F. *Soft Matter* **2008**, *4*, 1172–1177.